RESEARCH ARTICLE | MAY 03 2024

An investigation of self-interstitial diffusion in α-zirconium by an on-the-fly machine learning force field

Tan Shi ; Wenlong Liu; Chen Zhang; Sixin Lyu; Zhipeng Sun; Qing Peng; Yuanming Li; Fanqiang Meng ; Chuanbao Tang ; Chenyang Lu

AIP Advances 14, 055010 (2024)
https://doi.org/10.1063/5.0211883

An investigation of self-interstitial diffusion in α-zirconium by an on-the-fly machine learning force field

Cite as: AIP Advances 14, 055010 (2024); doi: 10.1063/5.0211883
Submitted: 2 April 2024 • Accepted: 19 April 2024 •
Published Online: 3 May 2024

Tan Shi,[1] Wenlong Liu,[2] Chen Zhang,[1] Sixin Lyu,[1] Zhipeng Sun,[3] Qing Peng,[4,5,6] Yuanming Li,[3] Fanqiang Meng,[2,a)] Chuanbao Tang,[3,a)] and Chenyang Lu[1,7,a)]

AFFILIATIONS

[1] School of Nuclear Science and Technology, Xi'an Jiaotong University, Xi'an 710049, China
[2] Sino-French Institute of Nuclear Engineering and Technology, Sun Yat-sen University, Zhuhai 519082, China
[3] Nuclear Power Institute of China, Chengdu 610213, China
[4] State Key Laboratory of Nonlinear Mechanics, Institute of Mechanics, Chinese Academy of Sciences, Beijing 100190, China
[5] Center of Materials Science and Optoelectronics Engineering, University of Chinese Academy of Sciences, Beijing 100049, China
[6] Guangdong Aerospace Research Academy, Guangzhou 511458, China
[7] State Key Laboratory of Multiphase Flow in Power Engineering, Xi'an Jiaotong University, Xi'an 710049, China

[a)] **Authors to whom correspondence should be addressed:** 383164381@qq.com; mengfq5@mail.sysu.edu.cn; and chenylu@xjtu.edu.cn

ABSTRACT

The on-the-fly machine learning force field approach, based on the Gaussian approximation potential and Bayesian error estimation, was used to study the diffusion of self-interstitial atoms in α-zirconium. *Ab initio* molecular dynamics simulations of lattice vibration and interstitial diffusion at different temperatures were employed to develop the force field. The radial and angular descriptors of the potential were further optimized to achieve better agreement with first-principles results. Subsequent long-term diffusion simulations were performed to assess the diffusion behavior based on the obtained force field. Tracer diffusion coefficients and diffusion anisotropy were studied at temperatures of 600–1200 K, and the Bayesian errors were estimated throughout the diffusion simulations. The mean and maximum estimated Bayesian errors of atomic force were approximately twice as large as those observed during the learning period. The basal diffusion was greatly favored compared to the interstitial diffusion along the c-axis, consistent with previous simulations based on first-principles results and classical potentials. The accuracy and applicability of the current on-the-fly machine learning approach were critically evaluated.

I. INTRODUCTION

Characterizing material behavior through machine learning force field (MLFF) typically requires an extensive dataset derived from first-principles calculations.[1–4] The generation of on-the-fly MLFF, facilitated by molecular dynamics (MD) simulations, offers a promising avenue to mitigate this challenge by automatic sampling of the configurational space and precise monitoring of extrapolation errors.[5–7] Such methodology is advantageous for addressing specific material behavior, especially when development of a comprehensive force field is unaffordable. However, when a specialized MLFF is constructed, its fidelity demands particular attention to ensure exhaustive sampling of the studied configurational space.

Defect diffusion behavior plays an important role in a material's physical and mechanical properties, material processing, and defect evolution under extreme environments. In this study, self-interstitial diffusion in α-zirconium was investigated with the on-the-fly MLFF approach to explore the possibility of constructing an accurate force field for interstitial diffusion, utilizing training data that primarily

originate from *ab initio* molecular dynamics (AIMD) simulations. Zirconium alloys are commonly used nuclear materials for commercial nuclear reactors.[8] Understanding the radiation defect evolution in α-zirconium is important for understanding the radiation growth of zirconium-based nuclear alloys.[9] Particularly, as α-Zr has an HCP structure, the diffusion anisotropy of self-interstitial atoms and self-interstitial clusters along the basal plane and the c-axis has a significant impact on the defect microstructure growth in different crystallographic planes.[10–12] Various locally stable interstitial configurations exist in α-Zr, including basal octahedral (BO), split dumbbell in the basal plane (BS), crowdion in the basal plane (BC), octahedral (O), split dumbbell along the c-axis (S), crowdion (C) configurations, among others, and they can exhibit very close stability in terms of energy.[13–15] The complicated migration pathways among these configurations compete with each other and determine the overall diffusion dynamics and diffusion anisotropy.

Although AIMD can accurately simulate interstitial diffusion, the limitation in diffusion time prevents obtaining statistically significant results with respect to the diffusion coefficient and diffusion anisotropy. The typical acceptable simulation time is on the order of ~100 ps for each temperature, which is generally not enough to collect a sufficient number of defect jumps. Based on the MLFF method, system energy, atomic force, and stress tensor can be directly learned from various configurations from AIMD simulations, and the diffusion time can be greatly extended. In this work, atomic vibration and interstitial diffusion at various temperatures were learned by the on-the-fly MLFF approach and long-term interstitial diffusion was simulated based on the obtained MLFF.

II. METHOD

Density functional theory (DFT) calculations were performed using the Vienna *ab initio* simulation package (VASP).[16,17] The on-the-fly MLFF was constructed within the VASP code using the Gaussian approximation potential (GAP).[18] The Bayesian linear-regression was used to optimize the potential and estimate the uncertainty.[19] During MD simulations, the decision to perform new AIMD calculations and update force field was according to a series of Bayesian error estimation (BEE)-based criteria. A comprehensive description of the MLFF theory can be found in Ref. 6.

To determine the DFT parameters and supercell size for the generation of on-the-fly MLFF AIMD training data, formation energies of typical α-Zr interstitial configurations (BO, BS, BC, O, S, and C configurations; see the Appendix for the initial interstitial structures) were compared under different simulation settings, including $5 \times 5 \times 3$ (150 atoms) and $4 \times 4 \times 5$ (180 atoms) supercells, $2 \times 2 \times 2$ and $3 \times 3 \times 3$ Γ-centered k-point meshes, and volume relaxation schemes of full relaxation and rescaled constant volume. In the rescaled constant volume scheme, the supercell volume was rescaled by $N/(N+1)$, where N is the total number of atoms in the perfect structure. The objective is to obtain the correct energy description of various interstitial configurations, given that these interstitial configurations are close in formation energies. In these DFT calculations, the Perdew–Burke–Ernzerhof generalized gradient approximation (PBE-GGA)[20] was used as the exchange-correlation functional. 12 electrons ($4s^2 4p^6 4d^2 5s^2$) were considered for the Zr atom. The electronic and ionic convergence thresholds were set to 10^{-4} eV and 0.01 eV/Å, respectively. A plane-wave cutoff of 400 eV was used. By comparing the interstitial formation energies from different DFT settings, a supercell size of 150 atoms with k-point meshes of $2 \times 2 \times 2$ was used for the following AIMD simulations for MLFF generation.

The dynamic simulations were performed using a Nosé–Hoover thermostat with a timestep of 2 fs. During the learning process, the perfect lattice vibration and self-interstitial diffusion were simulated for 20 and 40 ps, respectively, and this was performed sequentially at 1500, 1200, 900, and 600 K. High temperatures were used here to accelerate the diffusion and encompass as many potential local chemical configurations as possible. In this process, AIMD calculations were performed when the current atomic environment exceeded the BEE-based thresholds. Default machine learning (ML) descriptors, BEE thresholds, and weighting parameters were used during the on-the-fly learning. Static DFT results, including different interstitial configurations and compressive and tensile unit cells up to 15%, were also added to the training set. After the initial on-the-fly learning process, the obtained MLFF was refitted by adjusting the machine learning parameters to improve the force field accuracy. After the refitting of the MLFF, long-term interstitial diffusion simulations were then performed at different temperatures (600, 800, 1000, and 1200 K) with three 10-ns runs at each temperature. In these long-term diffusion simulations, only MLFF was performed without AIMD simulations.

III. RESULTS AND DISCUSSION

The interstitial formation energies with different DFT settings are presented in Fig. 1(a), with the corresponding data tabulated in Table I. It is known that when the supercell is small in α-Zr ($\lesssim$96 atoms), the lowest-energy configuration is incorrect.[14,15] The BO configuration should have the lowest formation energy; however, the O configuration becomes equally stable or more stable when using a small supercell. Previous DFT studies have indicated that supercell sizes of 180–200 atoms are needed to reflect the correct order of formation energies of various interstitial configurations.[14,15] Therefore, we compared the interstitial formation energies between supercell sizes of 150 atoms and 180 atoms using different k-point meshes to achieve a balance between energy accuracy and computational efficiency of AIMD simulations. In all the simulated cases presented in Table I, the BO configuration exhibits the lowest formation energy. The other interstitial configurations also show a consistent trend, with the order of formation energy being BO < BS < O < S ≈ C′. The C configuration is unstable and shifts to the C′ position by breaking the symmetry. The BC configuration is also unstable and is spontaneously relaxed to the BO configuration. The difference in formation energy between BO and O is slightly larger than that observed in previous studies. In most cases, the energy differences between BO and other interstitial configurations are consistent with previous DFT results, with differences of less than 0.1 eV. The observed discrepancy could be caused by different pseudopotentials, supercell sizes, and k-point meshes. The formation energies based on the rescaled constant volume are close to those with full volume relaxation (see Table I), with differences of less than 0.02 eV. Based on the good agreement among different DFT settings and previous results, the

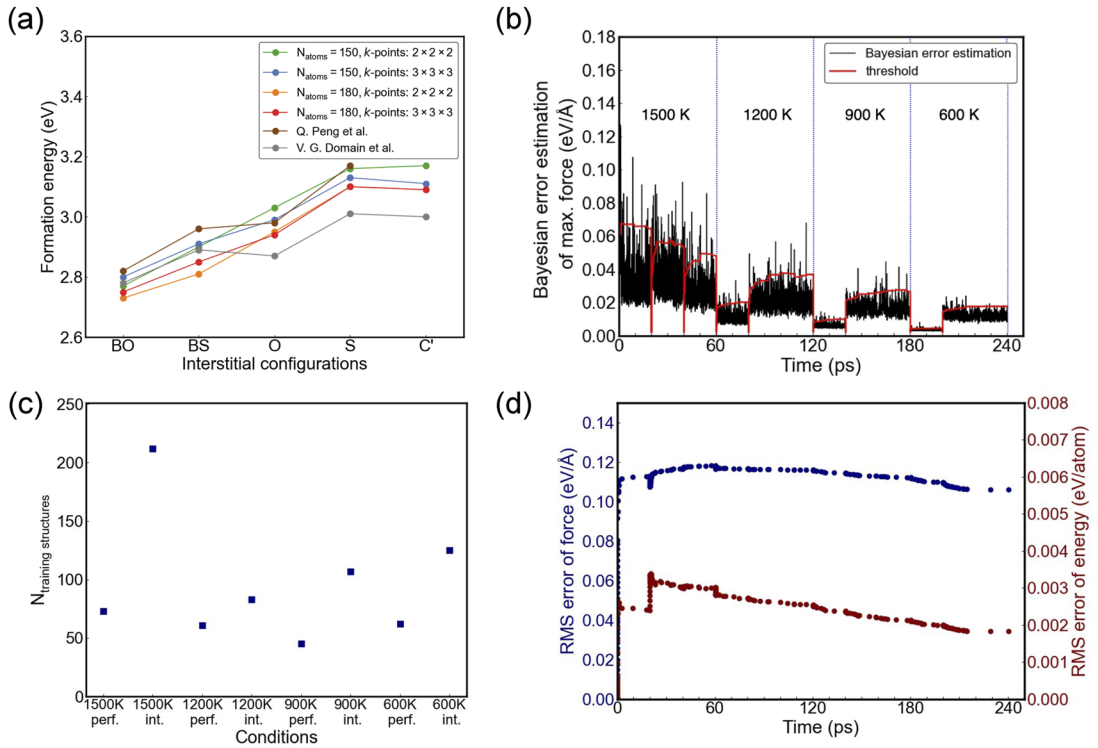

FIG. 1. (a) Interstitial formation energies with different DFT settings with the rescaled constant volume method. Previous DFT results are also presented.[14,15] (b) Evolution of Bayesian error estimation. For each temperature, 20 ps of perfect lattice vibration and 40 ps of interstitial diffusion were simulated. The BEE threshold is also presented in red. (c) Number of collected training configurations under each condition (perf.: perfect lattice vibration; int.: interstitial diffusion). (d) Evolution of the root mean square errors of force and energy.

150-atom supercell with k-point meshes of 2 × 2 × 2 was used for generating ML training data.

The Bayesian error was estimated throughout the learning period, as shown in Fig. 1(b). The Bayesian error can accurately represent the trend of the actual error despite its smaller magnitude.[6] The threshold for DFT calculation and MLFF reconstruction was dynamically varied using an average of Bayesian errors from recent steps. It can be seen that severe atomic vibrations lead to large Bayesian errors at high temperatures and that the Bayesian errors decrease as the temperature decreases. It is also noted that the Bayesian errors of perfect lattice vibration are smaller than those of interstitial diffusion due to the less extreme local chemical environment. The number of added training structures at each stage is presented in Fig. 1(c). 770 structures were collected in total, which is

TABLE I. Formation energies of different self-interstitial configurations in α-zirconium with different DFT settings.

N_{atoms}	k-points	Relaxation method	E_{BO} (eV)	E_O-E_{BO} (eV)	E_{BS}-E_{BO} (eV)	E_S-E_{BO} (eV)	$E_{C'}$-E_{BO} (eV)	Reference
150	3 × 3 × 3	Volume relaxation	2.79	0.19	0.09	0.31	0.31	
150	3 × 3 × 3	Rescaled volume	2.80	0.19	0.11	0.33	0.32	
150	2 × 2 × 2	Volume relaxation	2.76	0.26	0.11	0.37	0.39	
150	2 × 2 × 2	Rescaled volume	2.77	0.26	0.13	0.39	0.40	
180	3 × 3 × 3	Volume relaxation	2.75	0.19	0.09	0.30	0.31	
180	3 × 3 × 3	Rescaled volume	2.75	0.19	0.10	0.31	0.31	
180	2 × 2 × 2	Volume relaxation	2.72	0.22	0.07	0.35	0.35	
180	2 × 2 × 2	Rescaled volume	2.73	0.22	0.08	0.37	0.36	
180	3 × 3 × 3	Rescaled volume	2.82	0.16	0.14	0.35		15
200	3 × 3 × 3	Rescaled volume	2.78	0.09	0.11	0.23	0.22	14

TABLE II. Performance of MLFF compared to DFT results. Comparison of average errors in energy and force against DFT training structures, and presentation of migration barriers and formation energy differences for various interstitial configurations.

	DFT	Default MLFF	Refitted MLFF
$\Delta E_{\text{training data}}$ (meV/atom)	···	1.77	0.92
$\Delta F_{\text{training data}}$ (eV/Å)	···	0.18	0.13
$E^{\text{m}}_{\text{BO-O}}$ (eV)	0.33	0.67	0.39
$E^{\text{m}}_{\text{BO-S}}$ (eV)	0.64	0.74	0.64
$E^{\text{m}}_{\text{BO-BS}}$ (eV)	0.27	0.36	0.37
E_{O}-E_{BO} (eV)	0.26	0.54	0.22
E_{S}-E_{BO} (eV)	0.37	0.18	0.29
$E_{\text{C}'}$-E_{BO} (eV)	0.39	0.51	0.33
E_{BS}-E_{BO} (eV)	0.11	0.37	0.38
E_{BC}-E_{BO} (eV)	0.00	0.00	0.00

significantly higher than the reference dataset for conventional potential fitting. A large number of interstitial structures were collected at 1500 K. A considerable number of configurations were also learned at lower temperatures, indicating the complexity of the local chemical environment during lattice vibration and interstitial diffusion. Compared to DFT training data, the root mean square (RMS) errors of force and energy are ~0.11 eV/Å and 2–3 meV, respectively [see Fig. 1(d)]. The RMS errors tend to decrease over time as the learning process progresses from high temperature (1200 K) to low temperature (600 K), with lower temperatures typically resulting in smaller RMS errors.

The obtained MLFF was further refitted to improve the accuracy before conducting long-term diffusion simulations. As indicated in Table II, the default MLFF has relatively large uncertainties in energy and force compared to the DFT training data. The interstitial formation and migration energies also differ from the DFT results. Although a significant number of atomic configurations can be identified through the current on-the-fly simulation settings, a more accurate GAP potential is required due to the small energy differences among various migration paths in α-Zr, which are on the order of ~0.1 eV.[13] For instance, according to DFT results, the migration barrier between BO and O is 0.33 eV, whereas the barrier between BO-BS is 0.27 eV. Refitting involves modifications of parameters of radial and angular descriptors,[21] which are presented in Table III. In total, 3312 local (atomic) reference configurations were used for the refitted potential. The average energy difference for the refined MLFF is <1 meV/atom, and the average force difference is 0.13 eV/Å for the training dataset. For the long-term interstitial diffusion simulations, the configurational space is similar to the training dataset. Therefore, a small deviation from the training data is important. In addition, most of the migration barriers and energy differences relative to the BO configuration closely align with DFT calculations (< 0.1 eV) (see Table II). However, a notable exception is observed in the case of E_{BS}, where the discrepancy is 0.27 eV. A further increase in basis functions in the descriptors does not seem to lower its energy state, and the refitted MLFF is already one order of magnitude less efficient than the original MLFF. It is important to recognize that interstitial configurations involve closely spaced atoms undergoing significant elastic deformation and that classical interatomic potentials of Zr also face challenges in achieving good energy agreement for all the interstitial configurations. Additional investigation is needed to study the possibility of accurately delineating the entire interstitial energy landscape. Nevertheless, the refitted MLFF exhibited reasonable accuracy and was used for the long-term diffusion simulations.

The long-term diffusion simulations were performed at temperatures of 600, 800, 1000, and 1200 K. The distributions of mean and maximum BEE are approximately twice as large as those from the learning stage at 600 and 1200 K, as shown in Fig. 2. The diffusion simulations at 800 and 1000 K were only performed with the refined MLFF so that no comparison can be made with the learning stage. The higher mean Bayesian errors in the prediction stage indicate that atomic configurations were not completely interpolated during the long-term diffusion simulations. The mean Bayesian error distribution increases steadily with the diffusion temperature. However, the maximum atomic Bayesian error at each timestep is maintained at approximately the same level across the studied temperature range, with a slight increase in the proportion at the high error end. This indicates that the maximum estimation errors are largely constrained within a definite range.

The atomic mean square displacement (MSD) was calculated using all atoms as tracers. Good linearity was observed between the MSD and diffusion time within the first half of the diffusion

TABLE III. Parameters used in the refitted machine learning force field.[21] The corresponding tags in the VASP code are also presented in parentheses.

Parameter	Value	Description
R_{cut1}	8.0	The cutoff radius for radial descriptor $\rho_i^2(r)$ (ML_RCUT1)
R_{cut2}	6.5	The cutoff radius for angular descriptor $\rho_i^3(r,s,\theta)$ (ML_RCUT2)
σ_{atom}	0.4	The standard deviation of the Gaussian functions used for broadening the atomic distributions (ML_SION1 and ML_SION2)
N_{R}^0	12	Number of radial basis functions used to expand the radial descriptor $\rho_i^2(r)$ (ML_MRB1)
N_{R}^l	10	Number of radial basis functions used to expand the angular descriptor $\rho_i^3(r,s,\theta)$ (ML_MRB2)
L_{max}	6	The maximum angular momentum quantum number of spherical harmonics used to expand atomic distributions (ML_LMAX2)
η_{l}	Off	Angular fitting on/off (ML_LAFILT2)

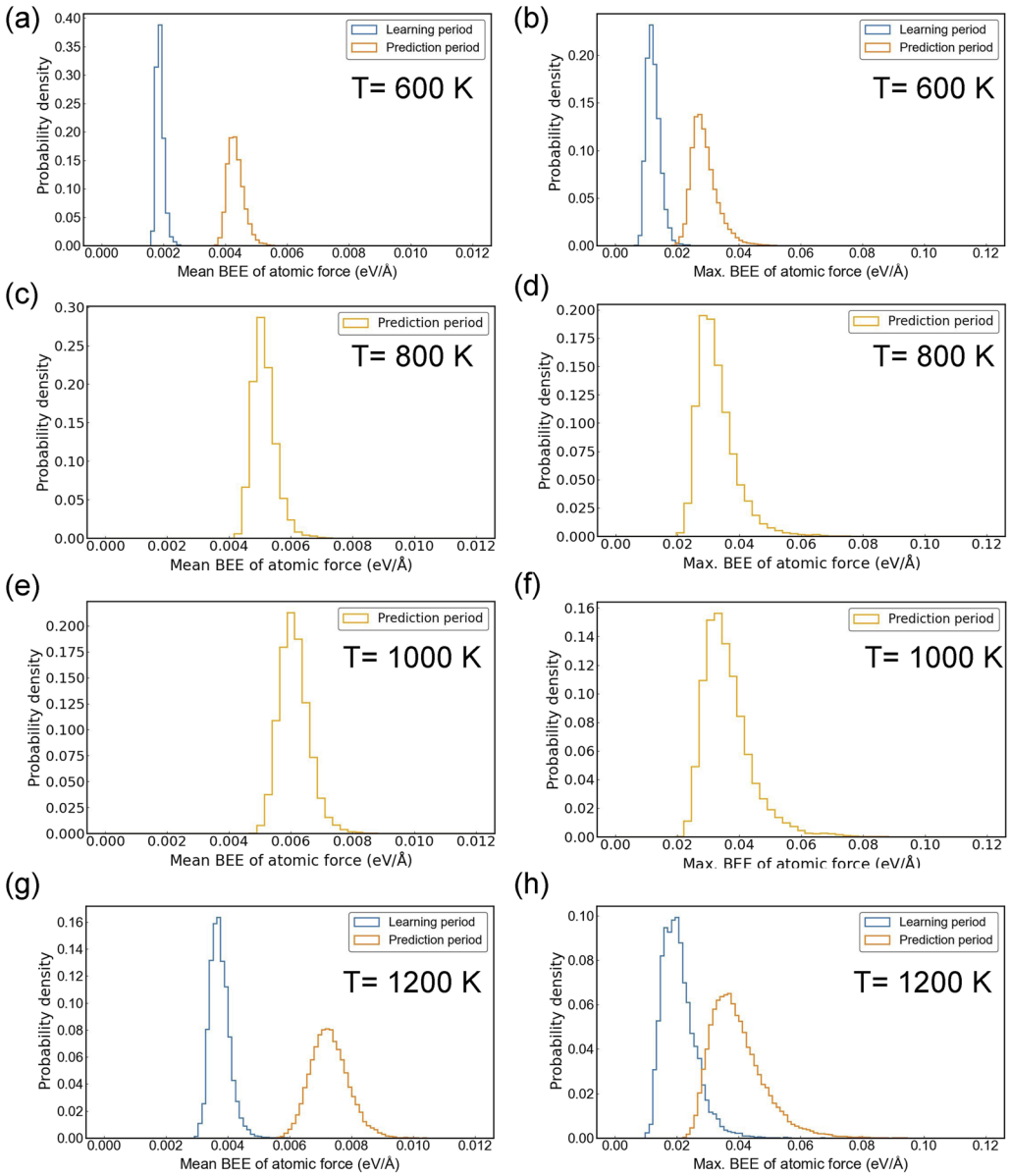

FIG. 2. Bayesian error estimation during the prediction period: distribution of mean and maximum BEE at [(a) and (b)] 600 K, [(c) and (d)] 800 K, [(e) and (f)] 1000 K, and [(g) and (h)] 1200 K. The Bayesian error estimation during the learning period was also shown for [(a) and (b)] 600 K and [(g) and (h)] 1200 K.

time difference (5 ns) for the studied temperature range over a period of 10 ns. The tracer diffusion coefficients were then calculated based on the first half of the MSD data: $D = MSD/(c_d \cdot 2nt)$, where c_d represents the interstitial concentration and n = 1, 2, and 3 for out-of-basal (D_c), basal (D_a), and total (D_t) diffusion coefficients, respectively. As shown in Fig. 3(a), the diffusion coefficients demonstrate an exponential relationship with 1/T. Anisotropic diffusion was observed with basal diffusion being significantly promoted. Based on the fitting to the Arrhenius relationship, the activation energies for D_c, D_a, and D_t are 0.38, 0.32, and 0.33 eV, respectively. With the classical potential of BMD07 developed by Wimmer *et al.*,[22] the c-axis and basal activation energies were found to be 0.30 and 0.17 eV, respectively.[23] For other classical potentials that predict the O configuration as the most stable configuration,[24,25] the diffusion dynamics are expected to be different.

The ratio D_a/D_c was found to decrease with increasing temperature [see Fig. 3(b)]. This trend aligns with results from Ref. 13, which were derived from Monte Carlo simulations of interstitial migration based on DFT migration barriers. Our results show that the magnitude of D_a/D_c is smaller with a higher decreasing rate with temperature.[13] In α-zirconium, the diffusion in the basal plane is primarily dominated by BO–BS migration, whereas the

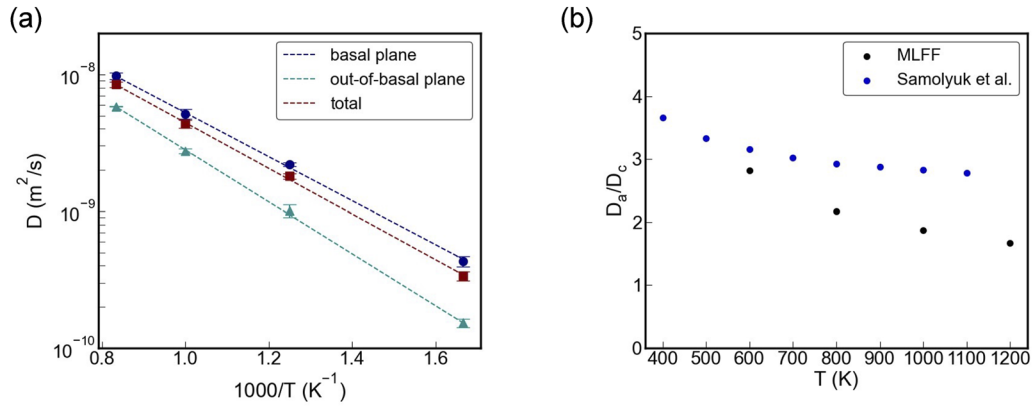

FIG. 3. (a) Tracer diffusion coefficient of the self-interstitial atom along different directions. (b) Ratio of D_a/D_c at different temperatures. Results from Samolyuk *et al.*[13] are also presented for comparison.

diffusion in the non-basal direction is primarily determined by BO–O migration. Migration paths that do not involve the most stable BO configuration, such as those among interstitial configurations of O, S, M, BS, etc., are also possible but are considered less prevalent. The overestimation of the BS energy state in the current MLFF may lead to variation in the diffusion anisotropy. In addition, our migration barrier between BO and O (0.22 eV) is slightly underestimated compared to our DFT result (0.26 eV), which promotes the diffusion along the c-axis and decreases the D_a/D_c value. Furthermore, we noticed that our DFT energies differ slightly from those obtained from Ref. 13. Since the MLFF is trained from our AIMD results, the difference in the obtained diffusion coefficient and diffusion anisotropy could also be attributed to the energy differences in the reference configurations. For instance, the M interstitial configuration, which was considered to be stable in Ref. 13, was found to be unstable in our DFT results. We also note a key difference when performing comparison with Refs. 13 and 23: In this work, tracer diffusion coefficients were determined, unlike the interstitial (defect) diffusion coefficients calculated in Refs. 13 and 23. The defect trajectory was also obtained using the Wigner–Seitz method to calculate the defect MSD. Despite conducting simulations over 30 ns at the same temperature, the statistical variation in the interstitial diffusion coefficient was found to be significant, rendering its calculation less reliable. Therefore, a further increase in computational efficiency is necessary with the MLFF method in order to get statistically convergent results on defect trajectories, particularly for the problem of diffusion anisotropy. Nevertheless, with the use of MLFF, the tracer diffusion coefficients and diffusion anisotropy can be determined based on a large dataset of interstitial diffusion configurations, greatly extending the timescale of *ab initio* MD simulations with moderate sacrifice in accuracy.

IV. CONCLUSION

The self-interstitial diffusion in α-zirconium was explored by the on-the-fly machine learning force field approach. The small energy differences among various migration paths in α-zirconium necessitate precise descriptions of all transition states and local energy minima. The developed force field explicitly accounted for various interstitial diffusion configurations at high temperatures and demonstrated reasonable accuracy in predicting interstitial properties. Strong diffusion anisotropy was observed in the basal direction, which is consistent with previous results based on DFT calculations and classical molecular dynamics simulations. Ensuring statistically significant diffusion coefficients requires an extended diffusion timescale. Potential improvement lies in the direction of accurately describing all defect energy states while preserving computational efficiency.

ACKNOWLEDGMENTS

We acknowledge the financial support from the National Key Research and Development Program of China (Grant No. 2022YFB1902402) and the LiYing Program of the Institute of Mechanics, Chinese Academy of Sciences (Grant No. E1Z1011001).

AUTHOR DECLARATIONS

Conflict of Interest

The authors have no conflicts to disclose.

Author Contributions

T. S. and W. L. contributed equally to this work.

Tan Shi: Conceptualization (equal); Data curation (equal); Formal analysis (equal); Investigation (equal); Methodology (equal); Project administration (equal); Writing – original draft (equal); Writing – review & editing (equal). **Wenlong Liu**: Data curation (equal); Formal analysis (equal); Investigation (equal). **Chen Zhang**: Data curation (supporting); Formal analysis (equal). **Sixin Lyu**: Formal analysis (supporting); Funding acquisition (supporting). **Zhipeng Sun**: Conceptualization (equal); Investigation (equal); Project administration (equal); Resources (equal); Supervision (equal); Writing – review & editing (equal). **Qing Peng**: Methodology (equal); Resources (equal); Software (equal); Writing – review & editing

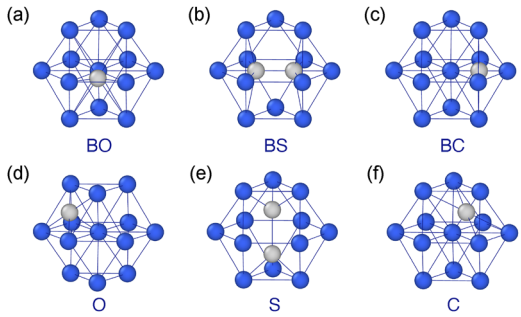

FIG. 4. Self-interstitial configurations in α-Zr: (a) BO configuration, (b) BS configuration, (c) BC configuration, (d) O configuration, (e) S configuration, and (f) C configuration.

(supporting). **Yuanming Li**: Conceptualization (equal); Methodology (equal); Project administration (equal); Resources (equal); Supervision (equal); Validation (equal); Visualization (equal); Writing – review & editing (equal). **Fanqiang Meng**: Conceptualization (equal); Formal analysis (equal); Methodology (equal); Resources (equal); Supervision (equal); Writing – review & editing (equal). **Chuanbao Tang**: Conceptualization (equal); Methodology (equal); Project administration (equal); Resources (equal); Supervision (equal); Validation (equal); Writing – review & editing (equal). **Chenyang Lu**: Conceptualization (equal); Project administration (equal); Resources (equal); Supervision (equal); Validation (equal); Writing – review & editing (equal).

DATA AVAILABILITY

The data that support the findings of this study are available from the corresponding authors upon reasonable request.

APPENDIX: SELF-INTERSTITIAL CONFIGURATIONS IN α-Zr

The various self-interstitial atom configurations are presented in Fig. 4, including basal octahedral (BO), split dumbbell in the basal plane (BS), crowdion in the basal plane (BC), octahedral (O), split dumbbell along the c-axis (S), and crowdion (C) configurations.

REFERENCES

[1] J. Byggmästar, K. Nordlund, and F. Djurabekova, Phys. Rev. Mater. **4**, 093802 (2020).
[2] H. Mei, L. Chen, F. Wang, G. Liu, J. Hu, W. Lin, Y. Shen, J. Li, and L. Kong, J. Nucl. Mater. **588**, 154794 (2024).
[3] D. Unruh, R. V. Meidanshahi, S. M. Goodnick, G. Csányi, and G. T. Zimányi, Phys. Rev. Mater. **6**, 065603 (2022).
[4] R. Jana and M. A. Caro, Phys. Rev. B **107**, 245421 (2023).
[5] V. L. Deringer, M. A. Caro, and G. Csányi, Adv. Mater. **31**, 1902765 (2019).
[6] R. Jinnouchi, F. Karsai, and G. Kresse, Phys. Rev. B **100**, 014105 (2019).
[7] C. Verdi, F. Karsai, P. Liu, R. Jinnouchi, and G. Kresse, Npj Comput. Mater. **7**, 156 (2021).
[8] R. Odette and S. Zinkle, *Structural Alloys for Nuclear Energy Applications* (Newnes, 2019).
[9] S. I. Choi and J. H. Kim, Nucl. Eng. Technol. **45**, 385 (2013).
[10] C. Woo, J. Nucl. Mater. **159**, 237 (1988).
[11] C. Woo and X. Liu, Philos. Mag. **87**, 2355 (2007).
[12] S. I. Golubov, A. V. Barashev, R. E. Stoller, and B. Singh, "Breakthrough in understanding radiation growth of zirconium," Technical Report (Oak Ridge National Laboratory (ORNL), Oak Ridge, TN, 2014).
[13] G. D. Samolyuk, A. V. Barashev, S. I. Golubov, Y. N. Osetsky, and R. E. Stoller, Acta Mater. **78**, 173 (2014).
[14] G. Vérité, C. Domain, C.-C. Fu, P. Gasca, A. Legris, and F. Willaime, Phys. Rev. B **87**, 134108 (2013).
[15] Q. Peng, W. Ji, H. Huang, and S. De, J. Nucl. Mater. **429**, 233 (2012).
[16] P. E. Blöchl, Phys. Rev. B **50**, 17953 (1994).
[17] M. Ernzerhof and G. E. Scuseria, J. Chem. Phys. **110**, 5029 (1999).
[18] A. P. Bartók, M. C. Payne, R. Kondor, and G. Csányi, Phys. Rev. Lett. **104**, 136403 (2010).
[19] C. Bishop, *Pattern Recognition and Machine Learning*, 2 (Springer, 2006), p. 531.
[20] J. P. Perdew, K. Burke, and M. Ernzerhof, Phys. Rev. Lett. **77**, 3865 (1996).
[21] J. Hafner, J. Comput. Chem. **29**, 2044 (2008).
[22] E. Wimmer, M. Christensen, W. Wolf, W. Howland, B. Kammenzind, and R. Smith, J. Nucl. Mater. **532**, 152055 (2020).
[23] J. F. March-Rico and B. D. Wirth, J. Nucl. Mater. **559**, 153441 (2022).
[24] M. I. Mendelev and G. J. Ackland, Philos. Mag. Lett. **87**, 349 (2007).
[25] S. Starikov and D. Smirnova, Comput. Mater. Sci. **197**, 110581 (2021).